Available online at www.sciencedirect.com
ScienceDirect
International Journal of Pharmaceutics 348 (2008) 125–136
INTERNATIONAL JOURNAL OF PHARMACEUTICS
www.elsevier.com/locate/ijpharm

Pharmaceutical Nanotechnology

Dirhenium decacarbonyl-loaded PLLA nanoparticles: Influence of neutron irradiation and preliminary in vivo administration by the TMT technique

Misara Hamoudeh [a], Hatem Fessi [a,*], Henri Mehier [b], Achraf Al Faraj [c], Emmanuelle Canet-Soulas [c]

[a] *Pharmaceutics and Pharmaceutical Technology Department, LAGEP, Laboratoire d'Automatique et de Génie de Procédés, UMR CNRS 5007, Université Claude Bernard (Lyon1) UCB, CPE-Lyon, Faculté de Pharmacie Lyon1,France*
[b] *Centre d'Etudes et de Recherches Médicales d'Archamps (CERMA), Domaine de Chosal, Archamps F-74160, France*
[c] *Université Lyon 1, CREATIS-LRMN, UMR CNRS 5220, CPE, La Doua, Villeurbanne, France*

Received 4 May 2007; received in revised form 9 July 2007; accepted 9 July 2007
Available online 14 July 2007

Abstract

In a previous study, we have described the elaboration of PLLA-based nanoparticles loaded with non radioactive dirhenium decacarbonyl [$Re_2(CO)_{10}$], a novel neutron-activatable radiopharmaceutical dosage form for intra-tumoral radiotherapy. These nanoparticles are designed for a neutron irradiation which can be carried out in a nuclear reactor facility. This new paper describes the neutron irradiation influence on these $Re_2(CO)_{10}$-loaded PLLA nanoparticles. The loaded nanoparticles with 23% (w/w) of metallic rhenium have shown to remain stable and separated and to keep out their sphericity at the lower neutron flux (1×10^{11} n/cm^2/s for 0.5 h) which was used for rhenium content determination (neutron activation analysis, NAA). However, when loaded nanoparticles were irradiated at the higher neutron flux (1.45×10^{13} n/cm^2/s, 1 h), they have shown to be partially coagglomerated and some pores appeared at their surface. Furthermore, DSC results showed a decrease in the PLLA melting point and melting enthalpy in both blank and loaded nanoparticles indicating a decrease in polymer crystallinity. In addition, the polymer molecular weights (M_n, M_w) decreased after irradiation but without largely affecting the polymer polydispersity index (P.I.) which indicated that an irradiation-induced PLLA chain scission had occurred in a random way. The XRD patterns of irradiated PLLA provided another proof of polymer loss of crystallinity. FTIR spectra results have shown that irradiated nanoparticles retained the chemical identity of the used $Re_2(CO)_{10}$ and PLLA despite the reduction in polymer crystallinity and molecular weight. Nanoparticles suspending after irradiation became also more difficult, but it was properly achievable by adding PVA (1%) and ethanol (10%) into the dispersing medium. Moreover, after 24 h incubation of different irradiated nanoparticles in two different culture mediums, visual examination did not show bacterial growth indicating that applied neutron irradiation, yielding an absorbed dose of 450 kGy, can be a terminal method for nanoparticles sterilisation. Thereafter, in a preliminary *in vivo* experiment, superparamagnetic non radioactive nanoparticles loaded with $Re_2(CO)_{10}$ and oleic-acid coated magnetite have been successfully injected into a mice animal model via targeted multi therapy (TMT) technique which would be our selected administration method for future *in vivo* studies. In conclusion, although some induced neutron irradiation damage to nanoparticles occurs, dirhenium decacarbonyl-loaded PLLA nanoparticles retain their chemical identity and remain almost as re-dispersible and injectable nanoparticles by the TMT technique. These nanoparticles represent a novel interesting candidate for local intra-tumoral radiotherapy.

Keywords: Rhenium; PLLA; Nanoparticles; Neutron irradiation; Polymer; Crystallinity; TMT; Cancer

1. Introduction

Nowadays, cancer is a major social and health issue. Cancer causes seven million deaths every year, corresponding to 12.5% of deaths worldwide (WHO website). Different cancer therapy strategies include combined or separated protocols of surgery, chemotherapy and radiotherapy. The radiotherapy can be realised by different approaches like; (i) external beam radia-

* Corresponding author at: Laboratoire Lagep, CPE Lyon, Bat 308G, 43 Bd du 11 Nov 1918, 69622 Villeurbanne cedex, France. Tel.: +33 4 72 43 18 93; fax: +33 4 72 43 16 82.
E-mail address: fessi@lagep.univ-lyon1.fr (H. Fessi).

0378-5173/$ – see front matter © 2007 Elsevier B.V. All rights reserved.
doi:10.1016/j.ijpharm.2007.07.010

tion, (ii) arterial embolization, (iii) metabolic radiotherapy, (iv) immunoradiotherapy and (v) brachytherapy (Chakarova et al., 2005; Alevizaki et al., 2006; Rivera et al., 2006; Andratschke et al., 2007; Hacker and Alken, 2007). With the exception of the first approach (i), the most promising trend is to treat the tumour area by delivering the radioactivity locally. External radiotherapy, unfortunately, destroy nearby healthy tissue along with the cancer cells resulting in various side effects or major complications (Buono et al., 2007). In order to reduce the morbidity rate of conventional radiotherapy and to enhance treatment effects on malignant tumours, it is highly desirable to accurately restrict the radiation to the localised tumour area. Among the above reported radiotherapy approaches, we distinguish the brachytherapy which is gaining actually an increased interest in oncology as an effective technique to deliver a radioisotope source as close as possible to the tumour site or directly into the tumour (Sun et al., 2005; Goh et al., 2007; Julow et al., 2007).

Among the different potential beta-emitting radioisotopes for brachytherapy we can find ^{90}yttrium, ^{166}holmium and $^{186\text{-}188}$rhenium. Recently, different research groups have investigated the incorporation of these isotopes in microparticles for radionuclide local delivery. The elaboration of these microparticles is generally realised using the isotopes being radioactive (Chunfu et al., 2004) or neutron-activatable (Nijsen et al., 2001). The substances that can be used to prepare these microparticles include albumin (Chunfu et al., 2004), resin (Wong et al., 2006) glass (Kim et al., 2006) and poly L-lactide (PLLA) (Nijsen et al., 2001). Interestingly, the PLLA, being a biodegradable and biocompatible polymer with interesting semi-crystalline properties, has been recently chosen as a matrix of microparticles, incorporating either (before their preparation) the neutron-activatable ^{165}holmium-complexes (Nijsen et al., 2001) or metallic $^{185\text{-}187}$rhenium (Hafeli et al., 2001) or being labelled (after their preparation) by the radioactive ^{90}yttrium (Hafeli et al., 1994) or a ^{188}rhenium salt (Chunfu et al., 2004). When the radioisotope is incorporated in its radioactive state, the second case, the nano(micro)particles have to be quasi-immediately administered to the patient to avoid the reduction of the radioactivity due to the radioisotope decay. This represents a disadvantage as it forces the manipulator to prepare on-site and on-demand the nano(micro)particles using a radioactive isotope. Hence, for a more practical application, it is preferable to prepare the nano(micro)particles in a neutron-activatable batch so that they can be ready at each moment for neutron activation for further programmed administration.

Neutron activation is actually carried out using nuclear reactors which yield high neutron fluxes up to 1×10^{14} n/cm^2/s. These high neutron fluxes enable higher activities to be attained in shorter activation times. For instance, glass-based microspheres (TheraSphere®, MDS Nordion, USA) including ^{90}yttrium are obtained by a neutron irradiation and used in primary liver cancer treatment. However, these glass microparticles are not biodegradable and may thus remain in the tissue long after the radioisotope has decayed (Hafeli et al., 2001). Furthermore, these microparticles have a high density rendering their injection problematic and raising problems of settling after injection (Herba et al., 1988). Therefore, and as mentioned above, the PLLA polymer has been selected as an alternative to prepare the nano(micro)particles for a subsequent neutron irradiation (Zielhuis et al., 2006; Hamoudeh et al., 2007a,b). Unfortunately, neutron irradiation together with the simultaneously generated gamma-rays can induce damage to the PLLA matrix (Hafeli et al., 2001; Nijsen et al., 2002). In a relatively similar context, a number of studies has addressed the effects of gamma irradiation used as a sterilization tool (25 kGy) on biodegradable polymers like PLLA and PLGA which are frequently used in drug delivery systems. It has been reported that these biodegradable polyesters undergo chain scission and crosslinking after exposure to γ-rays. Various works have reported a clear decrease in the PLLA or PLGA molecular weight after gamma irradiation (Spenlehauer et al., 1988; Sintzel et al., 1997; Lee et al., 2002). Researchers attributed this decrease to a dominant chain scission due to the resulting radicals' formation (Sintzel et al., 1997; Bittner et al., 1999; Martínez-Sancho et al., 2004). Chain scission occurs predominantly in the amorphous phase of the polymer (Mumper and Jay, 1992; Athanasiou et al., 1996). Similarly, this could imply that after a neutron irradiation in nuclear facilities, similar effects may be noticed in the PLLA matrix. However, irradiation in a nuclear reactor varies from γ-sterilisation (25 kGy) as the former yields a largely higher radiation doses reaching hundreds or thousands of kiloGrays (kGy) (Hafeli et al., 2001; Barbos, 2007).

Recently, we have described the elaboration of neutron-activatable $^{185\text{-}187}$dirhenium decacarbonyl [$Re_2(CO)_{10}$]-loaded PLLA nanoparticles for brachytherapy (Hamoudeh et al., 2007a,b). The nanoparticles have been prepared by an emulsion-evaporation method with a metallic rhenium loading of as high as 24% (w/w) which has been estimated to yield a suitable radiotherapeutic dose. Also, recently, Dr. Henri Mehier (Cerma, France) has invented a new promising technique for a multimodal intra-tumoral therapy and it was called Targeted Multi Therapy (TMT) (Hiltbrand et al., 2004). The first purpose of this technique is to treat solid tumours like brain, hepatic and pancreatic cancers by thermoablation which is carried out by the administration of hot vaporised water at 400 °C under a 400 bar pressure being attained by a hydropneumatic pump. The pulses of hot water vapour are injected though a microtube being perforated with several narrow halls of some microns (Roux et al., 2006). The efficacy of TMT technique-mediated thermonecrosis has already been proven for the treatment of cancers in animals (Hiltbrand et al., 2003, 2004). In this context, our anticipated strategy would be to combine two consecutive anticancer treatment modalities; in a first step, the thermoablation inducing a reduction of the tumour volume; and in a second step, the brachytherapy by a local injection of radioactive nanoparticles loaded with $^{186\text{-}188}$Re, via the same microtube.

The goal of this paper is to investigate the influence of neutron irradiation on dirhenium decacarbonyl [$Re_2(CO)_{10}$]-loaded PLLA nanoparticles using different techniques as scanning electron microscopy (SEM), gel permeation chromatography (GPC), differential scanning calorimetry (DSC), X-ray diffraction (XRD) and Fourier transform infrared spectroscopy (FT-IR). Finally, we show a feasibility experiment of the non

radioactive $Re_2(CO)_{10}$-loaded PLLA nanoparticles injection via the TMT technique mentioned above.

2. Materials and methods

2.1. Materials

Poly (L-lactide) PLLA (Resomer Condensate L M_n 1900 (M_w = 6 kDa)) was kindly supplied by Boehringer Ingelheim, Germany. Dirhenium decacarbonyl, poly(vinyl alcohol) (PVA, M_w = 31 kDa, hydrolyzation degree = 88%) and potassium bromide were all products of Aldrich, France. Dichloromethane (DCM) was from Laurylab, France. Nitric acid (65%), hydrochloric acid (12 M), sulphuric acid (95%) and ethanol were purchased from Carlo-Erba, France.

2.2. Nanoparticles preparation

$Re_2(CO)_{10}$-loaded nanoparticles were prepared by an oil-in-water simple emulsion-solvent evaporation method as described by Hamoudeh et al. (2007a,b) with modification. Briefly, the O/W emulsion consisted of:

- Organic phase: $Re_2(CO)_{10}$ was mixed with the polymer under different ratios in dichloromethane (DCM).
- Aqueous phase: PVA was used as a stabilizer in the external aqueous phase at a concentration ranging from 1 to 3% (w/v). The organic phase was then added into the aqueous one under mechanical stirring (Ultraturax T25, IKA, Germany) at a defined stirring speed for 2 min. The stirring speed ranged between 11,000 and 24,000 rpm.

After the emulsion formation, the DCM was evaporated by a rotative evaporator (R-144, Buchi, Switzerland) at 100 rpm for 15 min under vacuum. The prepared nanoparticles were separated by ultracentrifugation (Beckman, USA) and then washed with water for several times to eliminate the PVA excess.

Finally, 1 ml of NPs suspension was filled into 5 mL freeze-drying vials. The freeze-drying of nanoparticles was performed using a pilot freeze-dryer; Usifroid SMH45 (Usifroid, France). The conditions applied during the present study were: freezing for 2 h at −50 °C with a temperature ramp of 1 °C/min, sublimation at −40 °C and 60 μbar for 15 h and finally the secondary drying was carried out at 25 °C and 50 μbar for 4 h.

Furthermore, $Re_2(CO)_{10}$-loaded PLLA based superparamagnetic nanoparticles were prepared using the same above mentioned protocol except that 25 mg of oleic-acid coated magnetite were added to the organic phase and mixed with the polymer in an ultrasonic bath for 10 min (Hamoudeh et al., 2007a,b).

2.3. Rhenium loading and encapsulation efficacy determination

Two different methods were carried out to determine the rhenium content in nanoparticles.

2.3.1. Inductive coupled plasma atomic emission (ICP-AES)

Dirhenium decacarbonyl content was determined using a spectrometer ARL 3580 (Thermo, USA). A sample of about 20 mg of prepared nanoparticles was digested in a medium containing 1 volume of H_2SO_4 (95%) and 2 volumes of fuming HNO_3 (68%). The assay was linear between 0 and 10 μg (metallic rhenium)/ml with a correlation coefficient of 0.999. The encapsulation efficacy was calculated as following:

$$\text{Re}_2(\text{CO})_{10}\text{encapsulation efficacy } \% = 100 \times \left(\frac{\text{experimental loading}}{\text{theoretical loading}}\right)$$

2.3.2. Thermal neutron activation analysis (NAA)

This analysis has been carried out by bombarding the nanoparticles by a neutron flux of (1×10^{11} n/cm^2/s) for 30 min. The principle of this analysis is based on the fact that each formed radioactive nuclide during irradiation decays with a specific half-life, emitting gamma-rays of characteristic energy. Therefore, after irradiation, the gamma-ray induced activity in the samples is measured with a high resolution spectrometric system using high purity germanium (HpGe) detector. About five determinations have been carried out for each sample.

2.4. Size determination

The size of the $Re_2(CO)_{10}$-loaded nanoparticles was determined by a photon correlation spectroscopy (PCS) using Zetasizer 3000 HSa (Malvern, England) at 25 °C. Each measurement was performed in triplicate.

2.5. Scanning electronic microscopy

Irradiated and non-irradiated nanoparticles were deposited on a metallic probe then metallized with gold/palladium with a cathodic pulverizer (technics Hummer II, 6 V, 10 mA). Imaging was realized on a FEG Hitachi S800 SEM at an accelerating voltage of 15 kV.

2.6. Differential scanning calorimetry

Thermal analysis was performed using a differential scanning calorimeter DSC TA 125 (TA instrument USA). Five to ten milligrams of the samples were introduced into aluminium pans and hermetically sealed. All samples were heated at a 2 °C min^{-1} scanning rate between 25 and 200 °C after a 5 min stabilization plate under nitrogen atmosphere. The instrument was calibrated with indium for melting point and enthalpy heat of melting heat. For analysed samples, the glass transition temperature (T_g), the melting point (T_m) and the melting enthalpy were recorded. The polymer degree of crystallinity has been calculated as the percentage of its melting enthalpy over the melting enthalpy of a 100% crystalline PLLA ($\Delta H_{f(100\%)}$ = 95 J/g) (Sosnowski, 2002).

2.7. Gel permeation chromatography

Polymer molecular weights were determined on a Waters GPC system equipped with: an isocratic pump (Waters 515) operated at a flow-rate of 1 ml/min with tetrahydrofuran (THF), an autosampler (Waters 717 plus), a column oven and a refractive-index detector (RI) Model (Waters 410) with integrated temperature controller maintained at 35 °C. Data collection and data management were performed with the software ≪Empower pro≫ of Waters Corporation. For molecular mass separation a guard column (PLgel 5 μm), three Polymer Laboratories columns (2 × PLgel 5 μm Mixed C (300 × 7.5 mm)) and 1 PLgel 5 μm 500 A (300 × 7.5 mm)) were used in-line at 35 °C. Calibration was carried out using ND (narrow distributed)-polystyrene standards. The mobile phase was THF (HPLC grade) stabilized with dieter butyl-2,6 methyl-4 phenol. Polymer and nanoparticles samples were dissolved in THF, shortly sonicated in an ultrasonic bath to form a homogenous solution. Chromatography was carried out after sample filtration through a 0.45-μm. Toluene (internal standard) was added to standards and samples as a flow rate corrector.

Furthermore, as it has been established in literature, irradiations induce the formation and the breakdown of polymer bonds as a result of intermolecular crosslinking and chain scission, therefore, the radiation yields for chain scission (Gs) and cross-linking (Gx) have been determined and calculated from the following equations (Loo et al., 2005).

$$\frac{1}{M_w} = \frac{1}{M_{w0}} + \left(\frac{Gs}{2} - 2Gx\right) D \times 1.038 \times 10^{-6} \quad (1)$$

$$\frac{1}{M_n} = \frac{1}{M_{n0}} + (Gs - Gx) D \times 1.038 \times 10^{-6} \quad (2)$$

where M_{n0} and M_{w0} are number and weight average molecular weight before irradiation, M_n and M_w are the corresponding weights after irradiation and D is the absorbed dose (kGy).

2.8. X-ray diffraction

X-ray powder diffractometry analysis has been carried out using Siemens D500 apparatus operating with Cu Kα × radiation, a voltage of 40 kV and a current of 30 mA. The scans were conducted at a scanning rate of 1° min^{-1} in the 2θ range from 5° to 65°.

2.9. Fourier transformed infra-red spectroscopy

The nanoparticles, the polymer and $Re_2(CO)_{10}$ were characterised by infrared spectroscopy using a Unicam Mattson 5000 FT-IR spectrometer at room temperature. The spectra were taken in KBr discs in the range of 4500–400 cm^{-1}.

2.10. Nanoparticles re-dispersion after irradiation

A suspending test has been performed as described by Zielhuis et al. (2005) with some modifications. A sufficient amount of irradiated nanoparticles (around 10 mg) was weighed in an eppendorf tube (1.5 ml) tube and added to one of the following suspending mediums; saline, 1% PVA in saline, 10% ethanol in saline and 1% PVA in 10% ethanol in saline. To study the suspending behaviour, nanoparticles were vortexed for 1 min and it was examined visually whether a homogeneous suspension without aggregates was obtained. If this did not occur, the nanoparticles were further ultrasonicated for 1 min and again assessed visually.

2.11. Nanoparticle sterility

Gamma and neutron irradiated nanoparticles were transferred aseptically under laminar airflow conditions to vials containing 10 ml of (BHI, brain heart infusion) medium or (LB, Luria-Bertani) medium and were then left in incubation at 37 °C for 24 h. After 24 h, the tubes were tested visually.

2.12. Neutron irradiation

All irradiations were performed in the TRIGA reactor facilities in Pitesti, Institute for Nuclear Research, Romania. We used the irradiation channel with a thermal neutron flux of 1.45×10^{13} n/cm^2/s for 1 h. Irradiation was carried out in a sealed poly-propylene cylinder.

2.13. Gamma irradiation

Samples have been irradiated using a ^{60}Co-radiation source at 45 kGy at a rate of 11.28 kGy/h (Isotron, France).

2.14. In vivo injection of non-radioactive superparamagnetic $Re_2(CO)_{10}$-loaded nanoparticles via TMT technique

Six weeks old female OF1 mices were obtained from Charles River, France. Animals were housed in Lyon1 University animal-care unit, a facility accredited by the departmental direction of veterinary services. They had free access to conventional laboratory diet and water. The *in vivo* experiment was carried out in accordance with current French guidelines for the care of laboratory animals and was approved by the animal ethical committee of the Lyon1 University. Anaesthesia was maintained during the whole MRI process by 2% isoflurane delivered at 0.5 L/min. For MRI tests, mices were immobilized on a plastic bed, temperature was controlled by warm water circulating in a tube placed under the animal and respiration was monitored.

Six mices received an intramuscular injection in the left leg of 100 μl from a suspension of superparamagnetic non radioactive $Re_2(CO)_{10}$-loaded PLLA nanoparticles via the TMT technique mentioned above. Nanoparticles suspension has been prepared at a metallic iron concentration of 0.25 mMol which was estimated to be sufficient to allow following the local distribution of these nanoparticles being loaded with magnetite; a MRI negative contrast (Hamoudeh et al., 2007a,b).

MR imaging was carried out immediately after injection (D_0), the next day (D_1) and three days after (D_3). MRI was conducted

on a 4.7 T Bruker magnet (Bruker Biospin GmbH, Germany) interfaced to ParaVision software for preclinical MR imaging research. A Bruker transmission and reception RF coil tuned to the proton frequency was used. The applied sequence for analysis was a Gradient Echo sequence (TR/TE = 200/5 ms; 30° flip angle) at a resolution of 390 × 390 μm with four excitations to obtain a good signal-to-noise ratio. Gadolinium tubes (10^3 μM) positioned horizontally to mice were used to normalize the signal and allow a proper contrast-to-noise ratio analysis. Coronal slices (slice thickness = 2 mm) were positioned in order to image both mice legs and the gadolinium tubes.

Contrast to noise ratio (CNR) was calculated using Creatools software (Creatis-LRMN, France) on region of interest (ROI) where nanoparticles were located to compare and quantify their negative effect on MRI signal. The applied equation to calculate (CNR) was:

$$\mathrm{CNR} = \frac{(\mathrm{SNR_{Muscle}} - \mathrm{SNR_{ROI}})}{\mathrm{SNR_{Muscle}}} \text{with SNR} = \frac{\mathrm{Mean_{Signal}}}{\mathrm{S.D._{Noise}}} \quad (3)$$

where CNR, contrast to noise ratio; SNR, signal to noise ratio; S.D., standard deviation; ROI, region of interest where nanoparticles were located in D_0. This region was propagated in the other days and in the muscle of mice right leg.

3. Results and discussion

3.1. Preparation of $Re_2(CO)_{10}$-loaded nanoparticles and general properties

Dirhenium decacarbonyl [$Re_2(CO)_{10}$] has been chosen as a rhenium highly containing substance (56% (w/w) of rhenium) for encapsulation in poly(L-lactic acid) in order to obtain neutron-activatable nanoparticles. The applied method to prepare these nanoparticles was an oil-in-water emulsion-solvent evaporation method which showed to yield higher encapsulation efficiencies in comparison with other tried methods in our laboratory like the emulsion diffusion (data not shown). The different factors influencing the nanoparticles preparation have been extensively investigated in a previous study by an experimental design tool (Hamoudeh et al., 2007a,b). The nanoparticles size ranged between 330 and 1500 nm (Fig. 1) with a relatively small index of polydispersity (between 0.1 and 0.2) according to the photon correlation spectroscopy (PCS) results. The factorial design results attributed a clear negative effect for the stirring speed and the stabiliser concentration on the nanoparticles size while the polymer concentration exhibited a positive one (Hamoudeh et al., 2007a,b) in agreement with (Kwon et al., 2001; Sahoo et al., 2002; Hamoudeh and Fessi, 2006). Concerning the $Re_2(CO)_{10}$ encapsulation efficacy, the results showed the $Re_2(CO)_{10}$ encapsulation efficacy increasing at higher (lower) polymer (stabiliser) concentrations and also at slower stirring speeds in accordance with the results obtained concerning the encapsulation of lipophilic molecules (Gorner et al., 1999; Feng and Huang, 2001; El Bahri and Taverdet, 2007). The maximum rhenium loading, as a metal, was 24% by nanoparticles weight as determined by atomic emission assays and neutron activation analysis (Hamoudeh et al., 2007a,b).

The rhenium distribution within nanoparticles has shown to be homogenous as confirmed by the energy dispersive X-ray spectrometry (Hamoudeh et al., 2007a,b). Furthermore, FTIR experiments have not shown important interactions between PLLA and $Re_2(CO)_{10}$. Moreover, unlike other encapsulated molecules, the DSC assays demonstrated clearly that $Re_2(CO)_{10}$ has been encapsulated in its crystalline state (Hamoudeh et al., 2007a,b).

The neutron activation of these nanoparticles at a neutron flux of 1.45×10^{13} n/cm^2/s during 1 h yielded a specific activity of about 32.5 GBq g^{-1} of nanoparticles. This was estimated to be largely sufficient from a therapeutic point of view in taking into account the necessary elapsed time to ship the radioactive particles from the nuclear reactor facility towards the hospital (Hamoudeh et al., 2007a,b).

3.2. Irradiation effects on nanoparticles

3.2.1. Scanning electron microscopy

As it has mentioned above, the desired method for our nanoparticles administration would be an intra-tumoral injection by the targeted multi therapy technique invented by Dr. Mehier (Hiltbrand et al., 2004; Roux et al., 2006). This apparatus is equipped with a microtube perforated with narrow halls of only some microns. Therefore, we have chosen to encapsulate the neutron-activatable dirhenium decacarbonyl in nanoparticles (∼1 μm) rather than microparticles (Fig. 1). Here, we have investigated whether the size distribution and nanoparticles morphology had been modified after neutron irradiation. Indeed, the almost visible nanoparticles alterations because of neutron irradiations are due to the local absorbed heat by nanoparticles samples. Fig. 2(a, c) shows $Re_2(CO)_{10}$-loaded nanoparticles (23% rhenium (w/w)) after neutron irradiation at both neutron fluxes [1×10^{11} (Fig. 2a) and 1.45×10^{13} n/cm^2/s (Fig. 2c)]. It can be noticed that loaded nanoparticles kept out totally their spherical shape and remained separated at the lower neutron flux used for NAA determination while at the higher one, some nanoparticles appeared to be as misshaped spheres. In contrary, when comparing irradiated blank nanoparticles with $Re_2(CO)_{10}$-loaded nanoparticles, it appears that blank nanoparticles could bitter withstand the irradiations at 1.45×10^{13} n/cm^2/s for 1 h. Blank nanoparticles appear to be relatively aggregated as the loaded ones but the former ones kept out better their integrity while in the second case, a small part of loaded nanoparticles appears to have some pores on their surface (Fig. 2c). However, in both nanoparticles types, it seems in some micrograph parts that the PLLA polymer might start to melt at the point where nanoparticles touch each others. Indeed, Hafeli et al. (2001) have reported similar results for their PLLA-based microparticles (22 μm) loaded with 30% (w/w) rhenium metal after a quasi similar neutron irradiation conditions at 1.5×10^{13} n/cm^2/s during 1 h. According to authors, the theoretical temperature increase without heat transfer from the activation vial (poly-propylene cylinder) would be 238 K/h. This value has been obtained with the next equation supplied by

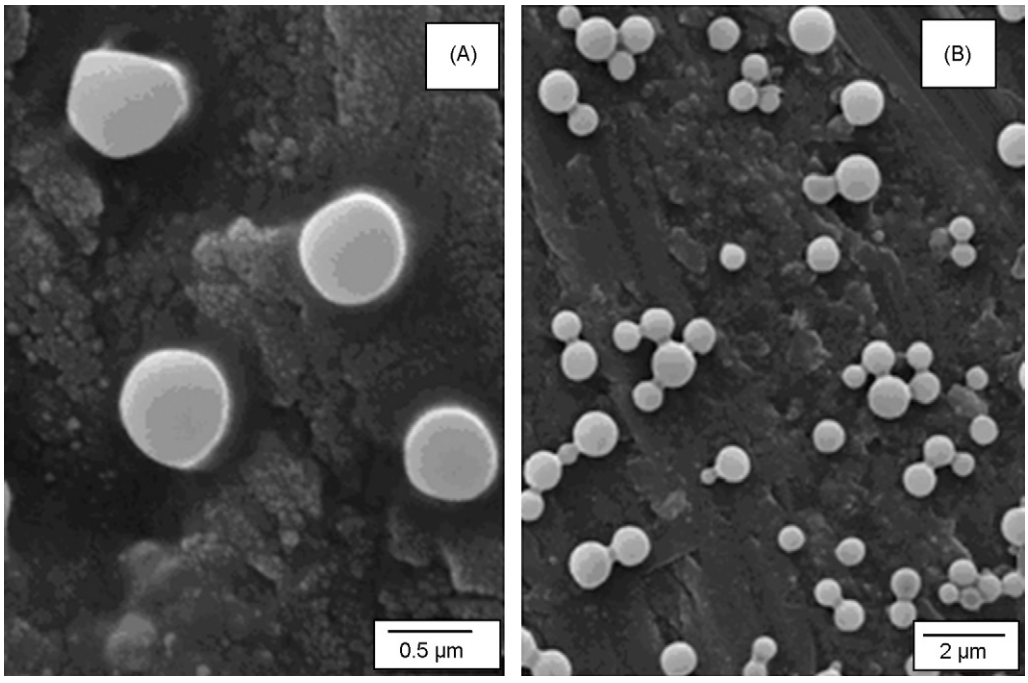

Fig. 1. SEM micrograph of dirhenium decacarbonyl-loaded nanoparticles before irradiation (bar = 0.5 μm (A), 2 μm (B)).

authors (4):

$$\frac{dT}{dt} = \frac{1}{c} \times \frac{dE}{dt} \quad (4)$$

where dT/dt is the temperature increase per second (K/s), the dE/dt is the energy deposited per kilogram per second (kJ/kg/s) and C is the PLLA specific heat value which is estimated to be 1.5 kJ/kg/K according to authors. Considering now that the local dose rate into our nanoparticles was 0.45 MGy/h (personal communication, Barbos, 2007) and that one Gray (Gy) equals 10^{-3} kJ/kg, thus the dose rate of 0.45 MGy/h equals 0.125 kJ/kg/s. By entering these data into Eq. (4) we calculated the temperature rise in our nanoparticles to be 0.0833 K/s or 300 K/h. However, as mentioned above in our study and that of Hafeli et al. (2001), it seems that the polymer melting point (here, $T_m = 142\,^{\circ}C$) has been reached as the polymer started to melt at the points where nanoparticles touch each others but without noticing a general melting of polymer. Therefore, we suggest that a heat transfer has occurred from the nanoparticles to the activation vial.

Furthermore, again in similarity with our results, Hafeli et al. obtained in the same study, microparticles with some pores at their surface. In our study, the pores formation was noticed only on $Re_2(CO)_{10}$-loaded nanoparticles while it was absent in blank nanoparticles. Therefore, we would support the authors' opin-

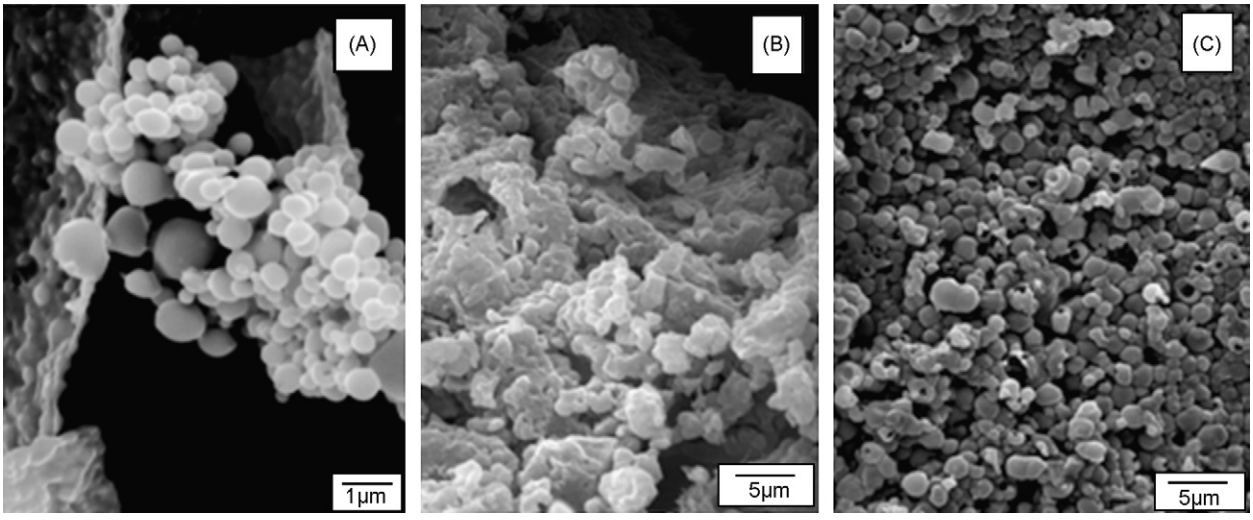

Fig. 2. SEM micrograph of (A) loaded nanoparticles after irradiation at 1×10^{11} n/cm^2/s for 30 min; (B) blank nanoparticles after irradiation at 1.45×10^{13} n/cm^2/s for 1 h; (C) loaded nanoparticles after irradiation at 1.45×10^{13} n/cm^2/s for 1 h (notice formed pores in some parts of Fig. 2C) (bar = 1 μm (A), 5 μm (B, C)).

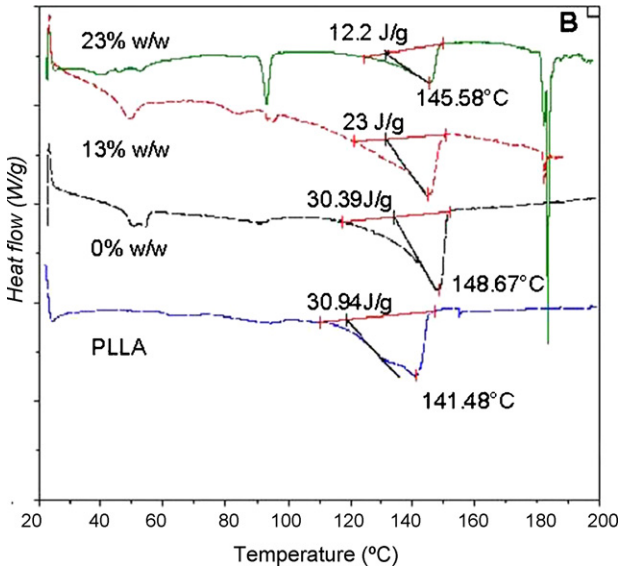

Fig. 3. DSC results of PLLA and nanoparticles loaded with 0, 13 and 23% (w/w) of metallic rhenium.

ion to explain this partial non generalized pore formation on our loaded nanoparticles. Indeed, pores formation may be due to the low specific heat value of rhenium which is 0.134 kJ/kg/K yielding by consequence a temperature increase of rhenium atoms of up to 0.93 K/s which is about 12 times more than that of PLLA (see above). Therefore, according to Hafeli et al. (2001) the rhenium atoms may represent some local hot spots in the PLLA matrix and lead consequently to the formation of some surface pores.

3.2.2. Polymer thermal properties

Representative DSC scans for $Re_2(CO)_{10}$ loaded and free nanoparticles are shown in Fig. 3. The pure $Re_2(CO)_{10}$ thermal curve displayed two separated sharp endothermic peaks at 93 and 170 °C corresponding respectively to a reversible transition and the $Re_2(CO)_{10}$ melting point as shown by Lemoine and Gross (1974) and Lemoine et al. (1975). The PLLA thermal curve showed a melting point at 142–143 °C with a melting enthalpy of 30 J/g indicating a semi-crystalline state with a degree of crystallinity of 31% which was calculated as the percentage of its melting enthalpy devised by the melting enthalpy for a 100% crystalline PLLA ($\Delta H_{f(100\%)} = 95$ J/g) (Sosnowski, 2002).

The PLLA melting enthalpy decreased from 31 to 23 to 12 J/g at rhenium metal loadings of 0, 13 and 23% (w/w), respectively (Hamoudeh et al., 2007a,b) which has been explained by a dilution effect due to the presence of ascending amounts of $Re_2(CO)_{10}$ within nanoparticles rather than a $Re_2(CO)_{10}$ plasticizer effect as shown by Mumper and Jay (1992) for holmium acetylacetonate-loaded PLLA nanoparticles.

The gamma irradiation (45 kGy) of or used PLLA and prepared nanoparticles induced a very small reduction in the PLLA melting point (becoming 141.4 °C) and a quasi negligible reduction of the melting enthalpy (becoming 28 J/g for PLLA polymer sample) which seems in agreement with the results of Zielhuis et al. (2006). However, after neutron irradiation at 1.45×10^{13} n/cm^2/s for 1 h, which can release a 0.45 MGy, both the PLLA melting point and melting enthalpy decreased in both blank and $Re_2(CO)_{10}$-loaded nanoparticles (23% w/w) to reach 136.8 °C and 17.5 J/g (for blank Np) and 120 °C and 4 J/g (for loaded Np) (Fig. 4, Table 1). The neutron irradiation-induced reduction of these two values for polymers like PLLA has been reported in literature reflecting a loss the polymer crystallinity and the presence of polymers with lower molecular weights (Cohn et al., 1987). For instance, Nijsen et al. (2001) reported a very sharp reduction of PLLA melting point from 176 to 147 °C and melting enthalpy from 25 to 4 J/g after the irradiation of holmium acetylacetonate-loaded PLLA microparticles (20–50 μm) at a neutron flux of 5×10^{13} n/cm^2/s for 0.5 h. Furthermore, Mumper and Jay (1992) indicated the same neutron irradiation influence on their holmium acetylacetonate-loaded PLLA microparticles (~7 μm). In their study, PLLA microparticles were irradiated at a 0.88×10^{13} n/cm^2/s and the PLLA melting point decreased from 173 to 78 °C and melting enthalpy from 38.3 to 4.3 J/g.

3.2.3. Polymer molecular weight

Table 2 summarizes the average molecular weights (M_w) and (M_n) in non irradiated, gamma irradiated (45 kGy) and neutron irradiated (450 kGy) PLLA, blank nanoparticles and $Re_2(CO)_{10}$-loaded nanoparticles.

Again, as reported for gamma or electron beam irradiation of PLLA (Merkli et al., 1994; Sintzel et al., 1997; Loo et

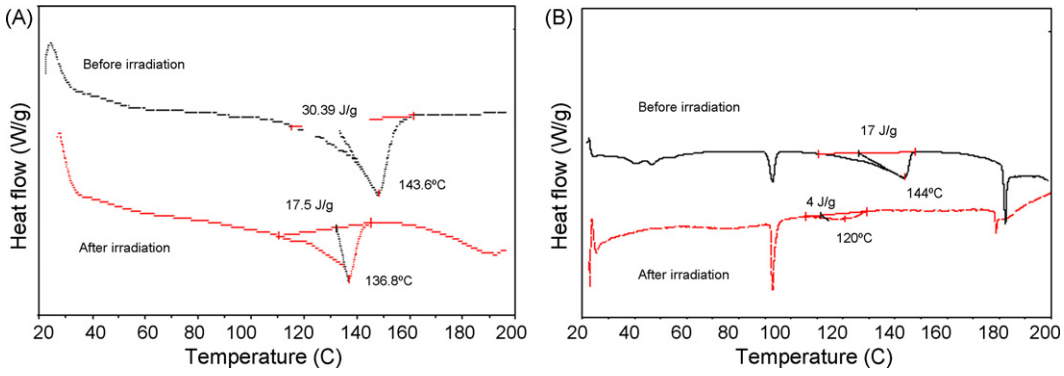

Fig. 4. DSC results of blank (A) and loaded nanoparticles (23%, w/w, metallic rhenium) (B) before and after neutron irradiation at 1.45×10^{13} n/cm^2/s for 1 h.

Table 1
DSC results of PLLA, blank and loaded nanoparticles before and after gamma irradiation (45 kGy) or neutron irradiation (450 kGy)

Sample	Before irradiation		After gamma irradiation (45 kGy)		After neutron irradiation (450 kGy)	
	T_m (° C)	Melting enthalpy (J/g)	T_m (° C)	Melting enthalpy (J/g)	T_m (° C)	Melting enthalpy (J/g)
PLLA	142	30	141.4	28	136	17.5
Blank nanoparticles	144	30.4	144	28	136.8	17.5
23% (w/w) loaded Nanoparticles	144	17	143.6	17.1	120	4

Table 2
GPC results of PLLA and loaded nanoparticles before and after gamma irradiation (45 kGy) or neutron irradiation (450 kGy)

Sample	Before irradiation			After gamma irradiation (45 kGy)			After neutron irradiation (450 kGy)		
	M_w (kDa)	M_n (kDa)	P.I.	M_w (kDa)	M_n (kDa)	P.I.	M_w (kDa)	M_n (kDa)	P.I.
PLLA	6.100	2.950	2.06	5.700	2.810	2.02	1.600	0.550	2.9
Nanoparticles	6.050	2.930	2.06	5.715	2.800	2.04	1.500	0.5	3

al., 2005) the neutron irradiation of nanoparticles resulted in a sharp decrease of the molecular weights reaching about 40% of the initial molecular weights in all samples. The neutron radiation yield values for chain scission (Gs) and cross-linking (Gx) have been determined from the Eqs. (1) and (2) (Section 2.7) and were found to be 3.95 and 0.08, respectively. This reflects that chain scissions are predominant over cross-linking when PLLA has been irradiated under our conditions. Furthermore, the polydispersity index (P.I. = M_w/M_n) has little increased after neutron irradiation indicating that the chain scission occurred in a random way (Sintzel et al., 1997; Loo et al., 2006; Milicevic et al., 2007). Indeed, the radiation-induced chain scissions of polymers like PLLA can occur by two mechanisms: (i) unzipping in which the terminal segments of polymer chains are preferentially cleaved inducing a decrease in the number average molecular weight (M_n) whilst the weight average molecular weight (M_w) is not largely affected (Gilding and Reed, 1979) and by consequence the polymer polydispersity index [P.I. = M_w/M_n] increases. (ii) A random fashion of polymer chains cleavage which leads to a reduction in both the M_n and M_w molecular weights and does not induce a very pronounced increase in the P.I. value (Chu and Campbell, 1982; Volland et al., 1994). In our opinion, our results are not compatible with an unzipping reaction as both the M_n and M_w molecular weights have been clearly reduced and the P.I. did only little increase. Therefore, in accordance with the results of Nijsen et al. (2002), we think that a random chain cleavage of the polymer chains is almost the principal cleavage reaction in the applied neutron irradiations conditions in our study.

3.2.4. X-ray diffraction

X-ray diffraction is a proven tool to study crystal lattice arrangements and yields useful information on samples degree of crystallinity. The diffraction profile for the PLLA revealed the presence of peaks at 14.8, 16.8, 19.1, and 22.9° being consistent with the peaks at 15, 16, 18.5, and 22.5° reported by Xu et al. (2006) and Ikada et al. (1987). After gamma and neutron irradiation, we noticed a decrease of these peak intensities (Fig. 5). This decrease has shown to be more pronounced after neutron irradiation indicating a decrease in the polymer crystallinity which is in accordance with the results of DSC.

3.2.5. Fourier transformed infra-red spectroscopy

Fig. 6 shows the FTIR spectra of both blank (Fig. 6A) and loaded nanoparticles (23% (w/w) metallic rhenium) (Fig. 6B) before and after neutron irradiation at 1.45×10^{13} n/cm^2/s during 1 h. The characteristic absorption peaks of PLLA are evident at 1750 cm^{-1} (carbonyl groups), 1080 cm^{-1} (C–O–C stretching bands) and 1450 cm^{-1} (C–H stretching in methyl groups) (Fig. 6A and B). The characteristic carbonyl-stretching band of $Re_2(CO)_{10}$ at 2071, 1992 and 1975 cm^{-1}, in accordance with the values given by Firth et al. (1986) were also detected in the nanoparticles indicating the stable nature of $Re_2(CO)_{10}$ after the encapsulation process (Fig. 6B). In both blank and loaded nanoparticles (Fig. 6A and B), after irradiation, the intensity of the peak at 3500 cm^{-1} increased corresponding to an increase in formed alcohol groups upon irradiation (Loo et al., 2004). Furthermore, in agreement with the results of Nijsen et al.

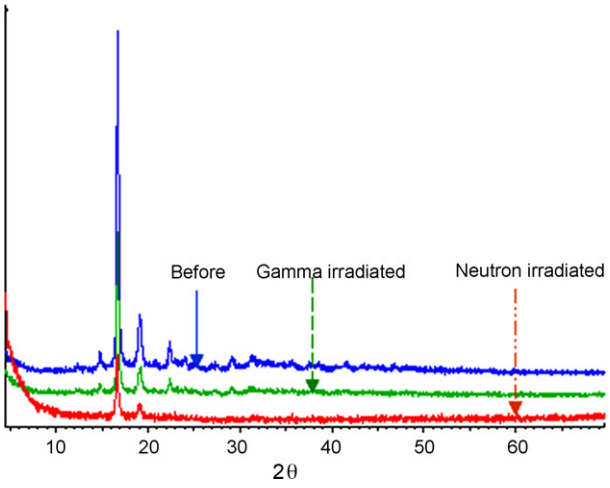

Fig. 5. XRD patterns of PLLA before and after gamma irradiation (45 kGy) or neutron irradiation (450 kGy).

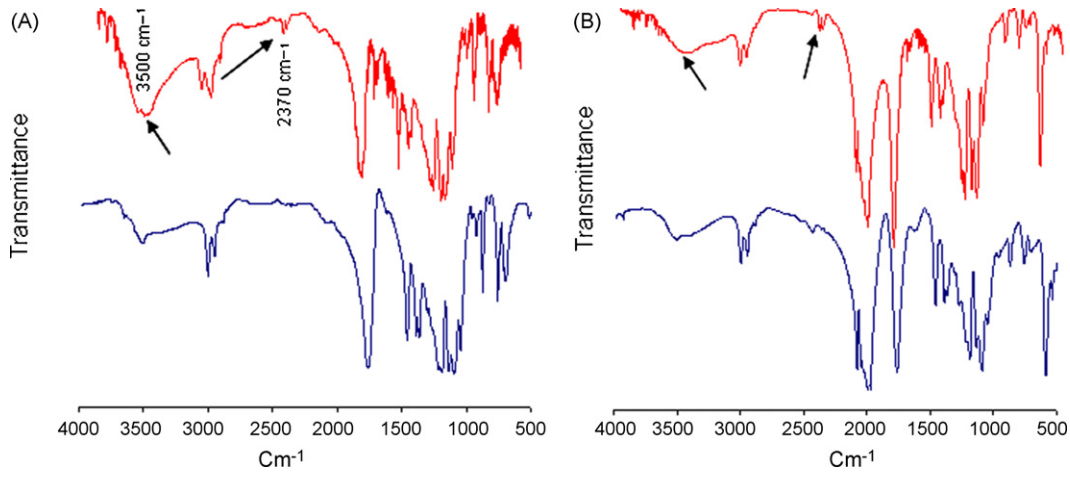

Fig. 6. FTIR spectra of blank (A) and loaded nanoparticles (23%, w/w, metallic rhenium) (B) before and after neutron irradiation at 1.45×10^{13} n/cm^2/s for 1 h.

(2002), we noticed an increase in the intensity of the broad peak ranged between 3200 and 3600 cm^{-1} corresponding to stretching vibrations of COOH end groups of PLLA chains due to chain scission confirming the results of GPC. Furthermore, a peak at 2370 cm^{-1} appeared in the spectra of irradiated samples indicating the presence of trapped carbon dioxide gas upon irradiation. However, again from figure, the retention of major peaks in PLLA spectra after irradiation (1750 cm^{-1}; carbonyl groups, 1080 cm^{-1}; C–O–C stretching bands and 1450 cm^{-1}; C–H stretching in methyl groups) (Lee et al., 1996; Paragkumar et al., 2006) and the carbonyl-stretching band of $Re_2(CO)_{10}$ at 2071, 1992 and 1975 cm^{-1} (Firth et al., 1986) provided a good proof that irradiated nanoparticles retained the overall chemical identity of the used $Re_2(CO)_{10}$ and PLLA in spite of PLLA molecular weight reduction.

3.2.6. Suspending behaviour of nanoparticles

Generally, we did not notice a difference in the suspending behaviour of lyophilized non-irradiated blank and $Re_2(CO)_{10}$-loaded nanoparticles in the different tried suspending mediums. After irradiation, it became more difficult to homogenously suspend nanoparticles. We suppose that this was due to some noticed nanoparticles agglomerations but as the nanoparticles administration would be by the TMT microtube being perforated with pores of some micrometers; this should not represent an obstacle for our nanoparticles' injection. However, good nanoparticles dispersions were well achievable by using 1% PVA in saline in presence of 10% ethanol.

3.2.7. Nanoparticles sterility

Different irradiated nanoparticles batches were incubated in (BHI) brain heart infusion medium or (LB) Luria-Bertani medium for 24 h. Visual examination after 24 h did not show bacteria growth in both mediums neither for gamma sterilised nanoparticles nor for neutron irradiated ones. Indeed, as it has been highlighted above, neutron irradiations under the applied conditions in our study can provide a 450 kGy absorbed dose for nanoparticles which is about 18 times higher than the frequently applied 25 kGy dose in gamma sterilisation. Therefore, in agreement with the results of Mumper and Jay (1992), we think that this nuclear reactor irradiation can yield radiotherapeutic nanoparticles and can serve as a final sterilisation method for our nanoparticles.

3.3. In vivo injection of non radioactive superparamagnetic $Re_2(CO)_{10}$-loaded nanoparticles via TMT technique (TMT injection feasibility)

The goal of this preliminary experiment has been to establish the possibility of nanoparticles injection via the TMT technique which would be our future desired treatment method. The injected nanoparticles were superparamagnetic $Re_2(CO)_{10}$-loaded ones which are loaded with magnetite crystals of 6 nm (4%, w/w, nanoparticles). The role of magnetite, being a negative contrast agent, in the composition of nanoparticles was to render them visible by magnetic resonance imaging (MRI). Indeed, one of the most known promising MRI is image-guided delivery of drugs in clinical oncology (Roullin et al., 2002; Seppenwoolde et al., 2005). The final iron concentration in nanoparticles suspension has been determined by ICP-AES and adjusted at 0.25 mM which was considered as a suitable concentration for MRI in a previous study (Hamoudeh et al., 2007a,b). The injection of nanoparticles suspension in the left leg of mices was carried out via the above introduced TMT microtube, being in turn perforated at its distal end with micrometric holes, under a 400 bar pressure being attained by a hydropneumatic pump (Hiltbrand et al., 2004). Fig. 7 shows the two legs of a mice immediately after injection (D_0), one day (D_1) and three days after (D_3). From Fig. 7, we notice that an area of a strong negative contrast in the left leg (the point of injection) which means that nanoparticles have been injected with success via the TMT technique and furthermore the high pressure of injection has allowed obtaining a localized nanoparticles zone. We think that this last point is very important because we aim in planned future *in vivo* experiments to obtain a radioactive zone of nanoparticles in the interior of tumour. We hypothize that it would be a potential mode of intra-tumoral treatment to irradiate tumour from such radioactive nanoparticles agglomerates zone. From Fig. 7 also, we notice that in the next day (D_1) we could localize the superparamagnetic nanoparticles preciously in the left leg while three

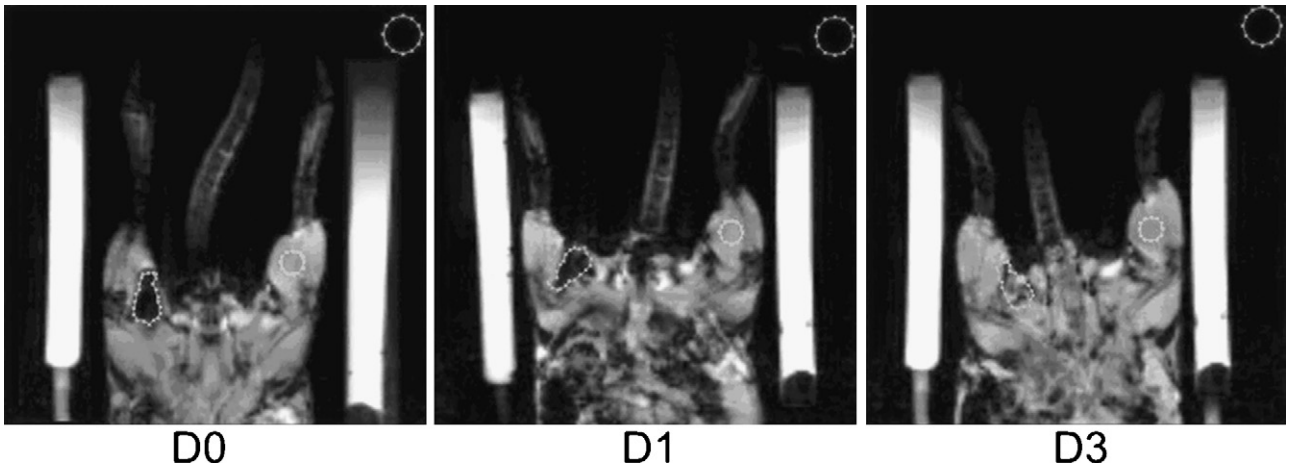

Fig. 7. MRI images of the two legs of a mice immediately (D_0), one day after (D_1) and three days after (D_3) injection of non radioactive superparamagnetic $Re_2(CO)_{10}$ nanoparticles (0.25 mM iron).

days after injection, the negative contrast was clearly lower and it seems that nanoparticles have been transported by the lymphatic network out from the injection area.

4. Conclusion

The mean objective of this paper is to describe the neutron irradiation impact on dirhenium decacarbonyl [$Re_2(CO)_{10}$]-loaded PLLA nanoparticles; a novel neutron-activatable radiopharmaceutical form for intra-tumoral radiotherapy. These nanoparticles were neutron irradiated in a nuclear reactor facility (Pitesti, Institute for Nuclear Research, Romania). The loaded nanoparticles with 23% (w/w) of metallic rhenium showed to remain stable and separated and to keep out their spherical shape at the lower neutron flux of 1×10^{11} n/cm^2/s (0.5 h) which was used for neutron activation analysis. In contrary, when loaded nanoparticles have been irradiated at the higher neutron flux (1.45×10^{13} n/cm^2/s, 1 h), nanoparticles showed to be partially coagglomerated and some pores appeared at their surface giving evidence that a local temperature increase in irradiation vials has occurred. Furthermore, DSC results demonstrated a reduction in PLLA melting point and melting enthalpy in both blank and loaded nanoparticles indicating a decrease in polymer crystallinity. In addition, PLLA molecular weights (M_n, M_w) decreased sharply after irradiation but without largely increasing the polymer polydispersity index (P.I.) which meant that an irradiation-induced PLLA chain scission has happened in a random way. Furthermore, XRD patterns of PLLA provided another proof of polymer crystallinity decrease. FT-IR spectra results have shown that the intensity of the peak at 3500 cm^{-1} increased corresponding to an increase in the formed alcohol groups due to chain scission upon irradiation. Moreover, FT-IR results showed that irradiated nanoparticles retained the overall chemical identity of $Re_2(CO)_{10}$ and PLLA although the recorded reduction in polymer crystallinity and molecular weight. Nanoparticle suspending behaviour after irradiation became also worse, but it was however possible to properly re-disperse irradiated nanoparticles by adding PVA (1%) and ethanol (10%) into the dispersing medium. Finally, in a preliminary *in vivo* experiment, superparamagnetic non radioactive $Re_2(CO)_{10}$-loaded nanoparticles have been successfully injected into a mice animal model via targeted multi therapy technique which would be our selected administration method for future *in vivo* studies. In conclusion, although neutron irradiation has induced some nanoparticles damage, dirhenium decacarbonyl-loaded PLLA nanoparticles retained their chemical composition and remain almost re-dispersible spheres with a suitable size distribution being adequate for TMT technique. We think that these nanoparticles represent a novel interesting radiopharmaceutical agent for an intra-tumoral radiotherapy.

Acknowledgments

The authors are grateful to Dr. Dumitru Barbos and Dr. Constantin Paunoiu from the Institute for Nuclear Research, Pitesti, Romania for the neutron irradiations of nanoparticles. Authors would thank Mr. Olivier Boyron from LCPP laboratory in Lyon1 University for GPC analysis and Professor Philippe Lejeune from (Laboratoire de Microbiologie, Adaptation et Pathogénie, INSA, Lyon) for the sterility test.

References

Alevizaki, C., Molfetas, M., Samartzis, A., Vlassopoulou, B., Vassilopoulos, C., Rondogianni, P., Kottou, S., Hadjiconstantinou, V., Alevizaki, M., 2006. Iodine 131 treatment for differentiated thyroid carcinoma in patients with end stage renal failure: dosimetric, radiation safety, and practical considerations. Hormones 5 (4), 276–287.

Andratschke, M., Gildehaus, F.J., Johannson, V., Schmitt, B., Mack, B., Reisbach, G., Lang, S., Lindhofer, H., Zeidler, R., Wollenberg, B., Luebbers, C.W., 2007. Biodistribution and radioimmunotherapy of SCCHN in xenotransplantated SCID mice with a 131I-labelled anti-EpCAM monoclonal antibody. Anticancer Res. 27, 431–436.

Athanasiou, A.K., Niederauer, G.G., Agrawal, C.M., 1996. Sterilization, toxicity biocompatibility and clinical application of polylactic acid/polyglycolic acid copolymers. Biomaterials 17, 93–102.

Barbos, B., 2007. Pitesti Nuclear Reactor, Institute for Nuclear Research Romania, personal communication.

Bittner, B., Mäder, K., Kroll, C., Borchert, H.H., Kissel, T., 1999. Tetracycline-HCl-loaded poly(DL-lactide-co-glycolide) microspheres prepared by a spray drying technique: influence of γ-irradiation on radical formation and polymer degradation. J. Controlled Release 59, 23–32.

Buono, S., Burgio, N., Hamoudeh, M., Fessi, H., Hiltbrand, E., Maciocco, L., Mehier-Humbert, S., 2007. Brachytherapy: state of the art and possible improvements. Anticancer Agents Med. Chem. 7 (4), 411–424.

Chakarova, A., Karanov, S., Petkova, E., Bakardjiev, S., Bogdanov, G., 2005. Brachytherapy after laser recanalization versus external beam radiotherapy after laser recanalization versus laser alone in inoperable oesophagocardial cancer: a controlled pilot study. J. BUON 10, 511–516.

Chu, C.C., Campbell, N.D., 1982. Scanning electron microscopic study of the hydrolytic degradation of poly(glycolic acid) suture. J. Biomed. Mater. Res. 16, 417–430.

Chunfu, Z., Jinquan, C., Duanzhi, Y., Yongxian, W., Yanlin, F., Jiaju, T., 2004. Preparation and radiolabeling of human serum albumin (HSA)-coated magnetite nanoparticles for magnetically targeted therapy. Appl. Radiat. Isot. 61, 1255–1259.

Cohn, D., Younes, H., Marom, G., 1987. Amorphous and crystalline morphologies in glycolic acid and lactic acid polymers. Polymer 28, 2018–2022.

El Bahri, Z., Taverdet, J.L., 2007. Elaboration and characterisation of microparticles loaded by pesticide model. Powder Technol. 172, 30–40.

Feng, S.S., Huang, G., 2001. Effects of emulsifiers on the controlled release of paclitaxel (Taxol®) from nanospheres of biodegradable polymers. J. Controlled Release 71, 53–69.

Firth, S., Hodges, P.M., Poliakoff, M., Turner, J.J., 1986. Comparative matrix isolation and time-resolved infrared studies on the photochemistry of $MnRe(CO)l0$ and $Re_2(CO)_{10}$ evidence for CO-Bridged $MnRe(CO)_9$. Inorg. Chem. 25, 4608–4610.

Gilding, D.K., Reed, A.M., 1979. Biodegradable polymers for use in surgery polyglycolic/poly(actic acid) homo and copolymers. Polymer 20, 1459–1464.

Goh, A.S., Chung, A.Y., Lo, R.H., Lau, T.N., Yu, S.W., Chng, M., Satchithanantham, S., Loong, S.L., Ng, D.C., Lim, B.C., Connor, S., Chow, P.K., 2007. A novel approach to brachytherapy in hepatocellular carcinoma using a phosphorous(32) ((32)P) brachytherapy delivery device-a first-in-man study. Int. J. Radiat. Oncol. Biol. Phys. 67, 786–792.

Gorner, T., Gref, R., Michenot, D., Sommer, F., Tran, M.N., Dellacherie, E., 1999. Lidocaine-loaded biodegradable nanospheres. I. Optimization of the drug incorporation into the polymer matrix. J. Controlled Release 57, 259–268.

Hacker, A., Alken, P., 2007. Therapy options in relapsing prostate cancer after external radiation therapy. Urologe A 46, 429–437.

Hafeli, U.O., Roberts, W.K., Pauer, G.J., Kraeft, S.K., Macklis, R.M., 2001. Stability of biodegradable radioactive rhenium (Re-186 and Re-188) microspheres after neutron-activation. Appl. Radiat. Isot. 54, 869–879.

Hafeli, U.O., Sweeney, S.M., Beresford, B.A., Sim, E.H., Macklis, R.M., 1994. Magnetically directed poly(lactic acid) 90Y-microspheres: novel agents for targeted intracavitary radiotherapy. J. Biomed. Mater. Res. 28 (8), 901–908.

Hamoudeh, M., Al Faraj, A., Soulas-Canet, E., Bessueille, F., Léonard, D., Fessi, H., 2007a. Elaboration of PLLA-based superparamagnetic nanoparticles: Characterization, magnetic behaviour study and in vitro relaxivity evaluation. Int. J. Pharm. 338 (1–2), 248–257.

Hamoudeh, M., Fessi, H., 2006. Preparation, characterization and surface study of poly-epsilon caprolactone magnetic microparticles. J. Colloid Interf. Sci. 300, 584–590.

Hamoudeh, M., Salim, H., Barbos, D., Fessi, H., 2007b. Preparation and characterization of radioactive dirhenium decacarbonyl-loaded PLLA nanoparticles for radionuclide intra-tumoral therapy. Eur. J. Pharm. Biopharm. 67, 597–611.

Herba, M.J., Illescas, F.F., Thirlwell, M.P., Boos, G.J., Rosenthall, L., Atri, M., Bret, P.M., 1988. Hepatic malignancies: improved treatment with intraarterial Y-90. Radiology 169, 311–314.

Hiltbrand, E., Belenger, J., Binzoni, T., Buchegger, F., Costa, M., Mehier, H., 2004. A new method of thermoablation with hot water vapour for localized tumours. Anticancer Res. 24, 2757–2763.

Hiltbrand, E., Belenger, J., Binzoni, T., Buchegger, F., Fessi, H., Costa, M., Quash, G., Foray, J., Mehier, H., 2003. Thérapie focalisée par micro-injections haute pression à l'aide d'un microtube implantable. ITBM-RBM 24, 136–144.

Ikada, Y., Jamshidi, K., Tsuji, H.O., Hyon, S.H., 1987. Stereocomplex formation between enantiomeric poly(lactides). Macromolecules 20, 904–906.

Julow, J., Szeifert, G.T., Balint, K., Nyary, I., Nemes, Z., 2007. Tissue response to iodine-125 interstitial brachytherapy of cerebral gliomas. Prog. Neurol. Surg. 20, 312–323.

Kim, D.Y., Kwon, D.S., Salem, R., Ma, C.K., Abouljoud, M.S., 2006. Successful embolization of hepatocelluar carcinoma with yttrium-90 glass microspheres prior to liver transplantation. J. Gastrointest. Surg. 10, 413–416.

Kwon, H.Y., Lee, J.Y., Choi, S.W., Jang, Y., Kim, J.H., 2001. Preparation of PLGA nanoparticles containing estrogen by emulsification-diffusion method. Colloid Surf. A 182, 123–130.

Lemoine, P., Gross, M., 1974. Decomposition Thermique du Dimanganese Decacarbonyle et du Dirhenium Decacarbonyle. J. Therm. Anal. Calorim. 6, 159–173.

Lemoine, P., Gross, M., Bousquet, J., Letoffe, M., Diot, M., 1975. Thermodynamic results on a solid-phase transition in dimanganese and dirhenium decacarbonyls. J. Chem. Thermodyn. 7, 913–917.

Lee, J., Isobe, T., Senna, M., 1996. Preparation of ultrafine Fe_3O_4 particles by precipitation in the presence of PVA at high pH. J. Colloid Interface Sci. 177, 490–494.

Lee, T.H., Wang, J., Wang, C.H., 2002. Double-walled microspheres for the sustained release of a highly water soluble drug: characterization and irradiation studies. J. Controlled Release 83, 437–452.

Loo, S.C.J., Ooi, C.P., Boey, Y.C.F., 2004. Radiation effects on poly(lactide-co-glycolide) (PLGA) and poly(L-lactide) (PLLA). Polym. Degrad. Stabil. 83, 259–265.

Loo, S.C.J., Ooi, C.P., Boey, F.Y.C., 2005. Degradation of poly(lactide-co-glycolide) (PLGA) and poly(L-lactide) (PLLA) by electron beam radiation. Biomaterials 26, 1359–1367.

Loo, S.C.J., Tan, H.T., Ooi, C.P., Boey, Y.C.F., 2006. Hydrolytic degradation of electron beam irradiated high molecular weight and non-irradiated moderate molecular weight PLLA. Acta Biomater. 2, 287–296.

Martínez-Sancho, C., Herrero-Vanrell, R., Negro, S., 2004. Study of gamma-irradiation effects on aciclovir poly(D,L-lactic-co-glycolic) acid microspheres for intravitreal administration. J. Controlled Release 99, 41–52.

Merkli, A., Heller, J., Tabatabay, C., Gurny, R., 1994. Gamma sterilization of a semi-solid poly(ortho ester) designed for controlled drug delivery-validation and radiation effects. Pharm. Res. 11, 1485–1491.

Milicevic, D., Trifunovic, S., Galovic, S., Suljovrujic, E., 2007. Thermal and crystallization behaviour of gamma irradiated PLLA. Radiat. Phys. Chem. 76 (8–9), 1376–1380.

Mumper, R.J., Jay, M., 1992. Poly(L-lactic acid) microspheres containing neutron-activatable holmium-165: a study of the physical characteristics of microspheres before and after irradiation in a nuclear reactor. Pharmacol. Res. 9, 149–154.

Nijsen, J.F.W., Van het Schip, A.D., Van Steenbergen, M.J., Zielhuis, S.W., Kroon-Batenburg, L.M.J., van de Weert, M., van Rijk, P.P., Hennink, W.E., 2002. Influence of neutron irradiation on holmium acetylacetonate loaded poly(L-lactic acid) microspheres. Biomaterials 23, 1831–1839.

Paragkumar, N.T., Edith, D., Six, J.L., 2006. Surface characteristics of PLLA and PLGA films. Appl. Surf. Sci. 253, 2758–2764.

Rivera, L., Giap, H., Miller, W., Fisher, J., Hillebrand, D.J., Marsh, C., Schaffer, R.L., 2006. Hepatic intra-arterial infusion of yttrium-90 microspheres in the treatment of recurrent hepatocellular carcinoma after liver transplantation: a case report. World J. Gastroentero. 12, 5729–5732.

Roullin, V.G., Deverre, J.R., Lemaire, L., Hindré, F., Venier-Julienne, M.C., Vienet, R., Benoit, J.P., 2002. Anti-cancer drug diffusion within living rat brain tissue: an experimental study using [3H](6)-5-fluorouracil-loaded PLGA microspheres. Eur. J. Pharm. Biopharm. 53, 293–299.

Roux, C., Rauber, N., Hiltbrand, E., Belenger, J., Khan, H., Dfouni, N., Michel, N., Knopf, J.F., Foray, J., Mehier, H., 2006. Experimental study on a large animal model of a new thermoablation technique. Anticancer Res. 26, 1–8.

Sahoo, S.K., Panyam, J., Prabha, S., Labhasetwar, V., 2002. Residual polyvinyl alcohol associated with poly (D,L-lactide-co-glycolide) nanoparticles affects

their physical properties and cellular uptake. J. Controlled Release 82, 105–114.

Seppenwoolde, J.H., Nijsen, J.F., Bartels, L.W., Zielhuis, S.W., Van Het Schip, A.D., Bakker, C.J., 2005. Internal radiation therapy of liver tumors: qualitative and quantitative magnetic resonance imaging of the biodistribution of holmium-loaded microspheres in animal models. Magn. Reson. Med. 53, 76–84.

Sintzel, M.B., Merkli, A., Tabatabay, C., Gurny, R., 1997. Influence of irradiation sterilization on polymers used as drug carriers. Drug Dev. Ind. Pharm. 23, 857–878.

Sosnowski, S., 2002. Poly(L-lactide) microspheres with controlled crystallinity. Polymer. 42, 637–643.

Spenlehauer, G., Vert, M., Benoit, J.P., Chabot, F., Veillard, M., 1988. Bioegradable cisplatin microspheres prepared by the solvent evaporation method: Mophology and release characteristics. J. Controlled Release 7, 217–229.

Sun, S., Qingjie, L., Qiyong, G., Mengchun, W., Bo, Q., Hong, X., 2005. EUS-guided interstitial brachytherapy of the pancreas: a feasibility study. Gastrointest. Endosc. 62, 775–779.

Volland, C., Wolff, M., Kissel, T., 1994. The influence of terminal gamma-sterilization on captopril containing poly(D,L-lactide-co-glycolide) microspheres. J. Controlled Release 31, 293–305.

Wong, C.Y., Savin, M., Sherpa, K.M., Qing, F., Campbell, J., Gates, V.L., Lewandowski, R.J., Cheng, V., Thie, J., Fink-Bennett, D., Nagle, C., Salem, R., 2006. Regional yttrium-90 microsphere treatment of surgically unresectable and chemotherapy-refractory metastatic liver carcinoma. Cancer Biother. Radiopharm. 21, 305–313.

Xu, H., Teng, C., Yu, M., 2006. Improvements of thermal property and crystallization behaviour of PLLA based multiblock copolymer by forming stereocomplex with PDLA oligomer. Polymer 47, 3922–3928.

Zielhuis, S.W., Nijsen, J.F., Figueiredo, R., Feddes, B., Vredenberg, A.M., Van het Schip, A.D., Hennink, W.E., 2005. Surface characteristics of holmium-loaded poly(L-lactic acid) microspheres. Biomaterials 26 (8), 925–932.

Zielhuis, S.W., Nijsen, J.F., Dorland, L., Krijger, G.C., van Het Schip, A.D., Hennink, W.E., 2006. Removal of chloroform from biodegradable therapeutic microspheres by radiolysis. Int. J. Pharm. 315 (1–2), 67–74.